ACS APPLIED MATERIALS & INTERFACES

Research Article

www.acsami.org

Solid Electrolytes for Fluoride Ion Batteries: Ionic Conductivity in Polycrystalline Tysonite-Type Fluorides

Carine Rongeat,*[,†] M. Anji Reddy,[†] Raiker Witter,[†,‡] and Maximilian Fichtner[†,§]

[†]Institute of Nanotechnology (INT), Karlsruhe Institute of Technology (KIT), Hermann-von-Helmholtz-Platz 1, 76344 Eggenstein-Leopoldshafen, Germany

[‡]Technomedicum, Tallinn University of Technology, Ehitajate tee 5, 19086 Tallinn, Estonia

[§]Helmholtz Institute Ulm for Electrochemical Energy Storage (HIU), Albert-Einstein-Allee 11, 89081 Ulm, Germany

Supporting Information

ABSTRACT: Batteries based on a fluoride shuttle (fluoride ion battery, FIB) can theoretically provide high energy densities and can thus be considered as an interesting alternative to Li-ion batteries. Large improvements are still needed regarding their actual performance, in particular for the ionic conductivity of the solid electrolyte. At the current state of the art, two types of fluoride families can be considered for electrolyte applications: alkaline-earth fluorides having a fluorite-type structure and rare-earth fluorides having a tysonite-type structure. As regard to the latter, high ionic conductivities have been reported for doped LaF_3 single crystals. However, polycrystalline materials would be easier to implement in a FIB due to practical reasons in the cell manufacturing. Hence, we have analyzed in detail the ionic conductivity of $La_{1-y}Ba_yF_{3-y}$ ($0 \le y \le 0.15$) solid solutions prepared by ball milling. The combination of DC and AC conductivity analyses provides a better understanding of the conduction mechanism in tysonite-type fluorides with a blocking effect of the grain boundaries. Heat treatment of the electrolyte material was performed and leads to an improvement of the ionic conductivity. This confirms the detrimental effect of grain boundaries and opens new route for the development of solid electrolytes for FIB with high ionic conductivities.

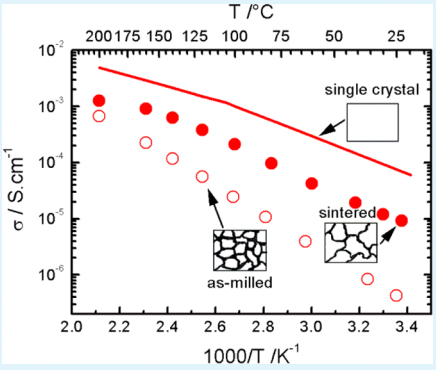

KEYWORDS: *Energy storage, ionic conductors, impedance spectroscopy, point defects, ball milling, solid electrolyte*

1. INTRODUCTION

Energy storage is one of the key steps in establishing the energy transition from fossil fuels to renewable energies. In particular, efficient electricity storage, i.e., in batteries, is needed to buffer the energy production cycles of renewable sources and also for mobility applications. Li-ion batteries are a mature and advanced technology,[1,2] and new research directions[3,4] are aiming at further improvements of the battery performance. Therefore, alternative technologies are investigated based on different chemistries using, for example, sodium,[5] magnesium[6] or chloride[7] as charge transfer ions in secondary batteries.

Recently, the principle of a secondary battery based on a fluoride shuttle (fluoride ion battery, FIB) was demonstrated.[8] Depending on the electrochemical couple, theoretical energy densities are offered of more than 5000 $Wh{\cdot}L^{-1}$. A critical component to obtain good cycling properties of the FIB is the electrolyte, which should provide fast F anion conduction. Solid electrolytes operating at elevated temperatures can be used for that purpose.[9] The high ionic conductivity of certain fluoride salts has been studied for a long time already.[10−13] The conductivity depends strongly on the structure of the fluoride, which determines the type of defects (F anion interstitials or vacancies) involved in the migration process through the crystals.[9,14,15]

Two types of fluoride families show particularly high ionic conductivity and are suitable for battery applications: compounds having fluorite-type (*Fm*-3*m*) or tysonite-type (*P*-3*c*1) structures. Alkaline-earth (Ca, Ba, Sr) fluorides have a fluorite-type structure and some of the rare-earth fluorides (RF_3 with R = La, Ce, Pr and Nd) show a tysonite-type structure. A large variety of compositions has been investigated, mostly single crystals of doped fluorite- or tysonite-type fluorides. However, it has also been found that polycrystalline compounds can have high conductivities, especially when having a nanostructure.[16,17] In a previous work, we studied in detail the conductivity mechanism in nanostructured $Ba_{1-x}La_xF_{2+x}$ solid solutions having a fluorite-type structure.[18] We demonstrated that the high conductivity is governed by the migration of vacancies along the grain boundaries that provide fast migration paths. Nanocrystalline compounds prepared by ball milling had higher conductivity than single crystals of the same compositions. We also reported that for the compound $La_{0.9}Ba_{0.1}F_{2.9}$ having a tysonite-type structure, the conduction mechanism is different as the presence of grain boundaries

Received: November 19, 2013
Accepted: January 20, 2014
Published: January 20, 2014

   dx.doi.org/10.1021/am4052188 | ACS Appl. Mater. Interfaces 2014, 6, 2103−2110

appears detrimental for ionic conduction. The aim of the present study is to perform a detailed study of the conductivity mechanism in $La_{1-y}Ba_yF_{3-y}$ solid solutions and to better understand the role of the grain boundaries.

Among tysonite-type fluorides, the highest conductivities have been reported for single crystals of LaF_3- and CeF_3-based solid solutions (e.g., 1.2×10^{-2} S·cm^{-1} for $La_{0.95}Sr_{0.05}F_{2.95}$ and 1.5×10^{-2} S·cm^{-1} for $Ce_{0.98}Sr_{0.02}F_{2.98}$ at 400 K (127 °C)[19]). For pure LaF_3, the conductivity is slightly anisotropic with a higher conductivity in the direction parallel to the *c*-axis than perpendicular to it.[11] The anisotropy disappears for higher temperatures or after doping LaF_3 with aliovalent fluorides. In addition, in the tysonite-type structure, F anions are located in three nonequivalent positions, F1, F2 and F3, and participate differently to the conduction mechanism. The ratio of F atoms in the different positions is 12:4:2 for F1, F2 and F3, respectively. However, the F2 and F3 positions show in fact very similar behavior and are often treated as structurally and dynamically equivalent (F2+F3 subsystem).[20]

The formation of F interstitials in a tysonite-type crystal is very unlikely because the interstitials sites in the tysonite-type structure are very small (0.84 Å and for F anion, radius is 1.19 Å).[21] The intrinsic defects in the tysonite-type structure are rather Schottky defects (cation vacancy associated with anion vacancy) and the anion conduction is a vacancy mechanism, which is different to what has been described for doped fluorite-type BaF_2.[15,22] At low temperatures, the conductivity is controlled by the exchange of F vacancies among the F1 subsystem. The activation energy decreases above 400−450 K (130−180 °C), indicating a change in the conductivity mechanism with additionally exchanges of F vacancies between the F1 subsystem and the F2+F3 subsystem.[19,20,23] However, mobility in the F2+F3 subsystem itself remains small. At even higher temperatures, above 700 K (420 °C), the activation energy increases again and the conduction mechanism involves F anions exchanges between all three positions F1, F2 and F3.[20,24]

As for the fluorite-type compounds, the conductivities are drastically improved by doping. Most of the results published reports on $R_{1-y}M_yF_{3-y}$ single crystals (R = La or Ce and M = Ba, Sr or Ca), which are obtained by mixing RF_3 with MF_2 in different concentrations.[24,25] However, the solubility of dopant is limited in tysonite-type compounds (up to 10−15 mol %[26]). For reasons of electroneutrality, the introduction of bivalent cations leads to the formation of F vacancies. For low concentrations of dopant, the conductivity increases with *y* and the activation energy decreases. This is mainly related to the formation of an increasing number of defects which are free to migrate. The conductivity reaches a maximum at the percolation threshold (ca. $y = 0.07$ for BaF_2 in LaF_3).[21] From this value, the activation energy for ionic conduction remains somehow constant but the vacancy migration is hindered by the presence of too many vacancies, leading to the formation of defect clusters. Few works have been published on polycrystalline LaF_3. Sobolev et al.[27] have prepared $La_{0.8}Ca_{0.2}F_{2.8}$ by ball milling. This quantity of CaF_2 is actually above the solubility limit of CaF_2 in LaF_3. Different milling conditions were used using a planetary mill but the ionic conductivity was almost not affected by them. The conductivity values stayed close to 5×10^{-4} S·cm^{-1} at 200 °C, but the activation energy was higher than reported for doped LaF_3 single crystals. For fluorite-type fluorides as CaF_2, the conductivity measured for nanoparticles has been found higher than for the same material having larger grains.[16] On the contrary, for nanoparticles of LaF_3, the conductivity decreases and the activation energy increases compared to single crystals.[28]

Here, we investigate the ionic conductivity of $La_{1-y}Ba_yF_{3-y}$ ($0 \le y \le 0.15$) solid solutions prepared by ball milling. The combination of DC and AC conductivity analyses provides a better understanding of the conduction mechanism in tysonite-type fluorides. The blocking effect of the grain boundaries for such compounds is considered regarding the effect of grain size in the compounds and the improvement of the conductivity by the tuning of this grain size is discussed.

2. EXPERIMENTAL SECTION

a. Materials and Methods. *Sample Preparation.* To prepare the solid solutions, $La_{1-y}Ba_yF_{3-y}$ ($0 \le y \le 0.15$), we used ball milling of a mixture of $(1 - y)$ LaF_3 and *y* BaF_2. The starting powders were dried at appropriate temperatures in vacuum for several hours prior to milling. For all compositions, 12 h milling at 600 rpm in a Si_3N_4 vial (ball-to-powder ratio 12:1) was enough to obtain a single phase solid solution with a tysonite-type structure.

For sintering treatment, pellets (13 mm diameter, ca. 1 mm thickness) of $La_{0.9}Ba_{0.1}F_{2.9}$ powder were pressed in air and then dried in vacuum for several hours before being placed in a quartz tube under Ar atmosphere. The tube was heated to 800 °C at 20 °C·min^{-1} and the temperature was maintained for 2 h before cooling down.

X-ray Diffraction (XRD). XRD measurements were performed using a Bruker D8 Advance instrument with Cu Kα radiation. Rietveld refinement was performed using the MAUD (Materials Analysis Using Diffraction) software package developed by L. Lutterotti.[29]

Nuclear Magnetic Resonance (NMR). Powdered samples were filled into 1.8 mm rotors for ^{19}F-NMR magic angle spinning at 40 kHz on a Bruker Avance NMR spectrometer with ^{19}F resonance frequency of 338 MHz. 90°/180° pulse lengths of a home build 1.8 mm probe were adjusted with 180 W to 0.8/1.6 μs. Rotor synchronized Hahn-echo experiments were applied to diminish ^{19}F background. The experimental repetition time was set to 4 s. Around the rotor, the air temperature was set to 300, 310, 320, 330, 340, and 350 K, which resulted (because of heating due to spinning) in sample temperatures of 318, 327, 336, 345, 354 and 363 K. ^{19}F-spectra were referenced to NaF (aqueous solution).

Electrochemical Impedance Spectroscopy (EIS). Ionic conductivity was measured by impedance spectroscopy on 13 mm diameter pellets pressed at 10^5 N and coated with Au on both sides as ion-blocking electrodes. The thickness of the pellets was measured prior to each measurement and was close to 1 mm. For EIS measurements on sintered samples, the sintered pellets were directly coated with Au after heating. The measurements were performed between room temperature and 200 °C in dynamic vacuum using a Zahner IM6 device and a frequency range of 8 MHz to 1 Hz (10 mV amplitude). The impedance spectra were fitted using the software EIS Spectrum Analyser[30] using the equivalent circuits described in the Results and Discussion.

b. Analysis of the Conductivity. In solid electrolytes,[31] DC ionic conductivity appears due to the presence of defects and their migration through the crystal and may be written as follows:[32−34]

$$\sigma_{DC} = \frac{a^2 q^2 N f_h}{6kT} \quad (1)$$

with *a* as the hopping distance, *q* the electronic charge, *k* the Boltzmann constant, *T* the absolute temperature, N_c the charge carrier concentration and f_h the ion hopping rate. These two last parameters are temperature dependent and follow Arrhenius laws:

$$N_c = N_0 \exp(-\Delta H_0/kT) \quad (2)$$

$$f_h = f_0 \exp(-\Delta H_m/kT) \quad (3)$$

with N_0 as the carrier concentration at infinite temperature and ΔH_0 the enthalpy for creation of mobile charge carriers, f_0 the fundamental vibrational frequency in the lattice (also called attempt frequency: number of times per second the ion attempts to move[34]) and ΔH_m the migration enthalpy.

Combining these equations, we obtain

$$\sigma_{DC} = \frac{a^2 q^2 N_0 f_0}{6kT} \exp\left(-\frac{\Delta H_0 + \Delta H_m}{kT}\right) = \frac{\sigma_0}{T} \exp\left(-\frac{E_a}{kT}\right) \quad (4)$$

with σ_0 as the pre-exponential factor and E_a the activation energy.

Studies about ionic conductivity typically show plots of $\log(\sigma_{DC}T)$ versus $1/T$ and give the activation energy (slope) and the pre-exponential factor (intercept). Moreover, the analysis of the frequency dependent AC conductivity $\sigma(f)$ as a function of the temperature allows the determination of f_h, ΔH_m, ΔH_0, N_c, f_0, N_0. The method used for AC conductivity analysis has been described in a previous study.[18]

Ionic conductivity is often measured by EIS[35] in a blocking-electrodes setup. For polycrystalline ionic conductors, the impedance spectrum in the complex plane (Nyquist plot) is generally composed of two semicircles and a tail at low frequency.[16] The semicircle at higher frequencies is generally related to bulk phenomena, here ionic conduction in the grains, the second semicircle is related to conduction in the grain boundaries and the tail at low frequency to the polarization of the electrodes.[36,37] Each semicircle can be fitted using an equivalent circuit composed of a resistance and a capacitance in parallel, the tail can be described by a pure capacitance. To fit the complete impedance spectrum all these elements are connected in series. Experimentally, pure capacitances are seldom used because the semicircles obtained are often depressed and the tails are tilted straight lines. This is mainly due to surface roughness or nonuniform reaction rates. Thus, in equivalent circuits used to fit measured impedance spectra, capacitances are replaced by constant phase elements (CPE), which impedance is given by $Z^*(\mathrm{CPE}) = 1/Q(j\omega)^n$.

3. RESULTS AND DISCUSSION

a. Synthesis of Doped-LaF_3 Compounds. Samples of $La_{1-y}Ba_yF_{3-y}$ with y = 0, 0.05, 0.1 and 0.15 were prepared by ball milling. The XRD patterns of all samples are given in Figure 1. After 12 h of milling, only reflections corresponding

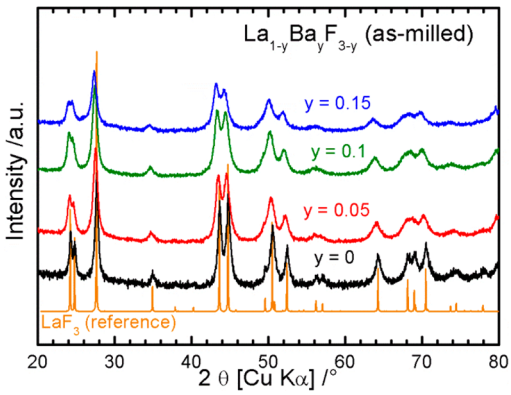

Figure 1. XRD patterns for ball-milled $La_{1-y}Ba_yF_{3-y}$ samples ($0 \le y \le 0.15$).

to a tysonite-type structure were obtained. The peak positions slightly shift to lower angles with the dopant content. The lattice parameters increase with y as expected because of the presence of an increasing amount of Ba^{2+} having a larger size than La^{3+}. The peaks obtained after ball milling were broadened because of the small crystallite size (10−20 nm) and the strain created during milling. The cell parameters and crystallite sizes determined by Rietveld refinement are given in Table 1.

Additional information about the different samples is given by NMR spectroscopy (Figure 2). The NMR spectrum for ball milled LaF_3 was composed of a single peak at −23.5 (−23.6) ppm of higher intensity than the double peak at 24.9 (25.3) ppm (with a shoulder at ca. 17 ppm), in agreement with earlier reports.[38,39] A BaF_2 peak would be expected around −14.3 ppm. The peak with higher intensity represents the F anions in F1 positions and the double peak represents the anions in F2 and F3 positions, which can hardly be distinguished. Unfortunately, here the relative peak integrals of F1 and F2+F3 alters from expected populations (ratio 12:4:2 for F1:F2:F3)[20] due to the usage of Hahn-echo experiment. The resulted peak ratios are influenced by the different relaxation behaviors of the different sites.

Nevertheless, the variation of the intensity ratios for different quantity of dopant indicates a change of the anion populations in the sites F1 and F2+F3, which is probably linked to the presence of vacancies.[20] The presence of these vacancies makes the exchange between the F1 and F2+F3 sublattices easier. This has already been reported considering the lower onset temperature found for a change of the conductivity mechanism from vacancies motion within the F1 sublattice only to the exchange between F1 and F2+F3 sublattices.[23] In addition, the peak position of F1 gives information about F1−F2+F3 exchange rates, which are in the range of 10^{-4}−10^{-6} s. Increased doping continuously shifts the F1 peak to higher frequencies, indicating a higher mobility.[20] The approach of F1 peak to F2+F3 peak reveals an easier exchange of anions between F1 and F2+F3 positions mostly because of the presence of an increasing number of defects. This gradual change in the chemical shift difference between the two peaks with increasing y has also been observed for doped-CeF_3 samples.[23]

b. Ionic Conductivity in the As-Milled Compounds. The DC ionic conductivity was calculated from the electrolyte resistance determined by EIS. The impedance spectra obtained for the different samples and at different temperatures were all composed of a semicircle at high frequency and a straight line at low frequency (Figure 3a,b). The spectra were all fitted using the equivalent circuit given in Figure 3c[18,40] and the results are given in Table S1 for the spectra at 30 °C (see the Supporting Information). The electrolyte resistance is given by the resistance of the semicircle at high frequencies. All corresponding capacitance values determined by fitting lie in the range corresponding to grain boundary phenomena.[36] At low frequencies, the straight lines are related to polarization phenomena at the interface electrolyte/electrodes.

The conductivities calculated from the electrolyte resistances at different temperatures are given in Figure 4 for all samples. The values of activation energy, E_a, and pre-exponential factor, σ_0, are obtained from eq 4 and given in Table 1. In this table are also given the values of migration enthalpy ΔH_m, defect formation enthalpy ΔH_0 and attempt frequency f_0 obtained from the AC analysis of the impedance results. For tysonite-type compounds, the hopping distances a can take different values because of the different F anion positions in the crystal.[21] It is therefore not straightforward to calculate the concentration of mobile defects according to eq 4.

For all compositions, the conductivity values are much lower than those reported for single crystals. This is mainly related to much higher activation energies (Table 1). Note that the

Table 1. Summary of the Crystal Structure Analysis and Conductivity Parameters for As-Milled $La_{1-y}Ba_yF_{3-y}$ Samples[a]

sample	$La_{1-y}Ba_yF_{3-y}$				$Ba_{0.6}La_{0.4}F_{2.4}$
y	0	0.05	0.1	0.15	
cell parameters (Å)	7.18	7.20	7.22	7.24	6.07
	7.35	7.37	7.39	7.41	
crystallite size (nm)	21	14	13	10	21
σ_{DC} at 160 °C (10^{-4} S·cm^{-1})	0.0165	0.993	2.81	2.05	1.88
E_a (eV)	0.26[b]	0.55	0.55	0.60	0.58
	0.66[c]				
σ_0 (10^5 S·K·cm^{-1})	6.10^{-7}[b]	1.56	3.54	9.50	4.90
	0.38[c]				
ΔH_m (eV)	0.26[b]	0.55	0.52	0.58	0.54
	0.66[c]				
ΔH_0 (eV)	0	0	0.03	0.02	0.04
f_0 (10^{13} Hz)	1.7×10^{-5}[b]	5.90	3.29	20.4	19.4
	10.1[c]				
E_a (eV) single crystal	0.46[d] (⊥)	0.37-0.38[d]	0.36-0.37[d]		0.58[e]
	0.43[d] (//)				

[a]The results obtained for fluorite-type $Ba_{0.6}La_{0.4}F_{2.4}$ are given for comparison.[18] [b]For T < 80 °C. [c]For T > 80 °C. [d]From ref 21 (⊥) conduction perpendicular to the c-axis, or (//) parallel to the c-axis, activation energies for x = 0.01−0.03 (average 0.02) and x = 0.06−0.09 (average 0.07). [e]From ref 18.

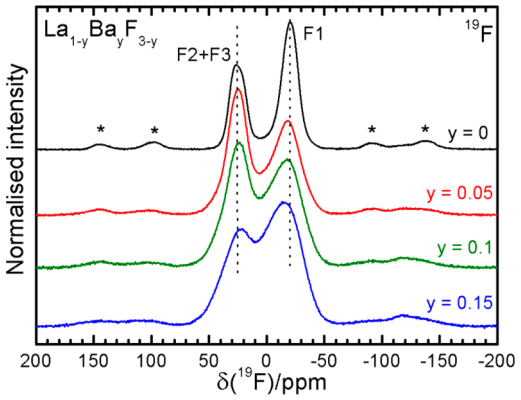

Figure 2. ^{19}F NMR spectra for $La_{1-y}Ba_yF_{3-y}$ ball-milled samples ($0 \leq y \leq 0.15$) at room temperature. The asterisks indicate the spinning side bands.

conductivity values given there are very reproducible between several pellets and several milling batch. The highest conductivity is obtained for the sample $La_{0.9}Ba_{0.1}F_{2.9}$. For pure ball-milled LaF_3, two regions in the Arrhenius plot can be seen with a change of slope around 80 °C. At low temperature, the activation energy is lower than at higher temperatures. This could indicate two different conduction mechanisms, but they appear to be opposite to what has been reported for single crystals (lower activation energies observed at higher temperatures).[25] However, for pure LaF_3 and at temperatures below 80 °C, the impedance spectra measured are highly distorted due to the very high impedance values measured (>10^6 Ω) and the limitations of our measuring instrument. It is therefore possible that some errors occurred during fitting because extrapolations are necessary and the electrolyte resistance could be underestimated. These results will thus not be discussed further here.

The values of activation energies are similar for all doped samples (0.55−0.60 eV) and are also similar to the values obtained for BaF_2-doped compounds.[18] NMR T_1-relaxation measurements, which mostly represent the signal dominating bulk core material gave much lower values in the range of 0.1−0.25 eV, which correspond to results from previous investigations.[20] This may be an indication that the conduction is also controlled by vacancies in the grain boundaries and would mean that the vacancies in the grain boundaries are not as fast as those present in the grains and created by doping. Unfortunately, fundamental studies about vacancies migration in tysonite-type fluorides are lacking so that the origin for this behavior remains unclear at the moment. It is possible that the vacancies in the grain boundaries are intrinsically not as mobile as those present in the grains, which could explain the comparable activation energies found for all ball-milled samples. Nevertheless, there should be some influence from the defects present in the grains as significant changes are found for the different compounds; the activation energies are always lower for the compounds having the lower activation energy in the single crystals. The mechanism of such an influence is not clear yet. In addition, the attempt frequency is also comparable in all samples pointing to a similar mechanism of conduction in all samples; the values determined here are typical for vibrations of the lattice 10^{12}−10^{13} Hz.[34] The activation energy and migration enthalpy are the lowest for $La_{0.9}Ba_{0.1}F_{2.9}$, which shows the highest conductivity values. The conductivity value decreases with higher dopant content as also reported for single crystals.[24] This is probably related to the formation of vacancies clusters which may affect the grain boundaries as well.

c. Effect of Sintering. Sintering of polycrystalline compounds is a common method to improve the ionic conductivity. This appears to be interesting for tysonite-type samples as the conductivity is rather slowed down by the grain boundaries. As a first study, two pressed pellets of $La_{0.9}Ba_{0.1}F_{2.9}$ (tysonite) and $Ba_{0.6}La_{0.4}F_{2.4}$ (fluorite) were heat treated at 800 °C for 2 h to promote grain growth. Additionally, for the sample $La_{0.9}Ba_{0.1}F_{2.9}$, one pellet was sintered for 20 h to study the effect of the sintering time. The conductivity was measured by EIS as described above. The XRD patterns of the sintered samples are given in Figure 5. The results of Rietveld refinements for these patterns are given in Table 2.

The increase in grain size is clearly seen in the XRD patterns by the sharpening of the diffraction peaks. Rietveld refinements gave a crystallite size larger than 70 nm for all samples. For the

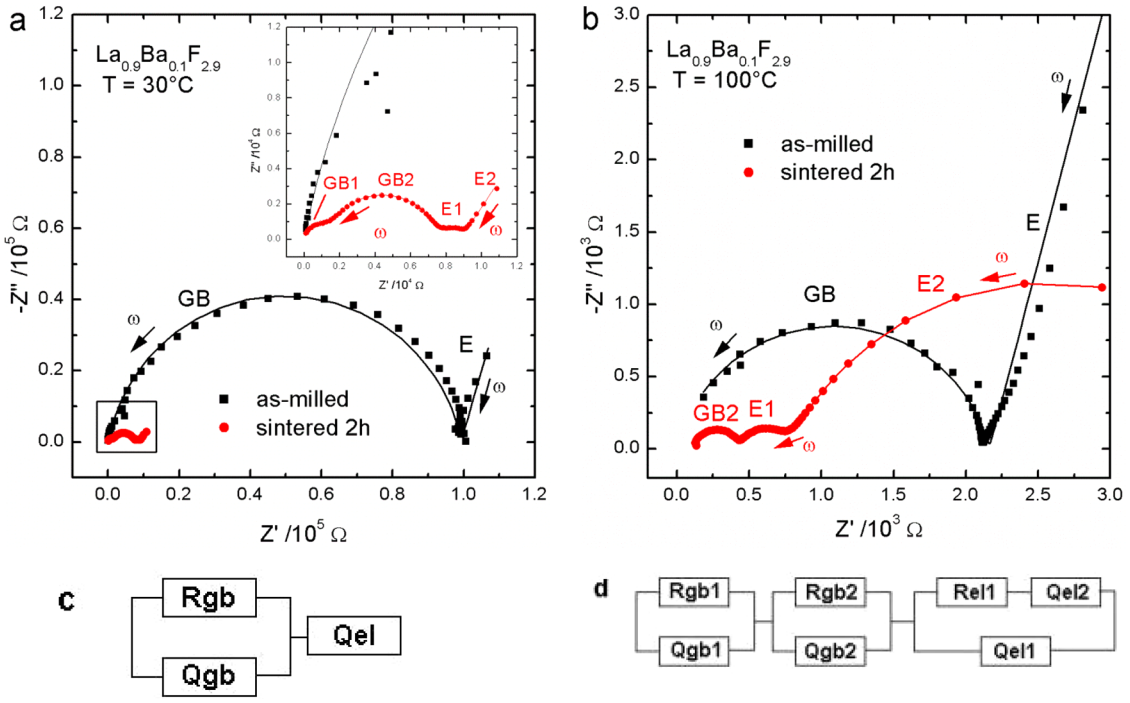

Figure 3. Complex plane plots obtained (a) at 30 °C (inset: enlargement of the low resistance area) and (b) at 100 °C for the samples $La_{0.9}Ba_{0.1}F_{2.9}$ as-milled and sintered for 2 h at 800 °C. The symbols represent the measured values and the lines are the fit obtained. Labels GB and E indicate sections of the spectra related to grain boundaries or electrode phenomena, respectively. (c and d) The equivalent circuits used for fitting the spectra obtained for as-milled and sintered samples, respectively.

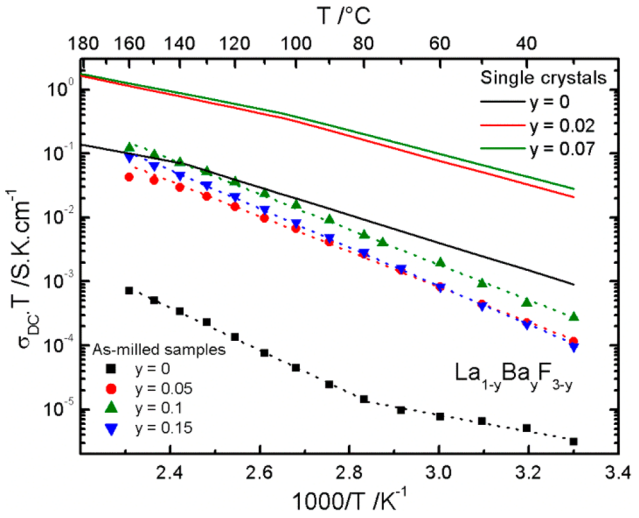

Figure 4. Arrhenius plot of the DC conductivity for $La_{1-y}Ba_yF_{3-y}$ samples prepared by ball milling. The values given for single crystals (solid lines) were taken from the literature for the conductivity along the *c*-axis (see also Table 1).[21] The dotted lines represent the linear fit obtained for calculating the activation energies.

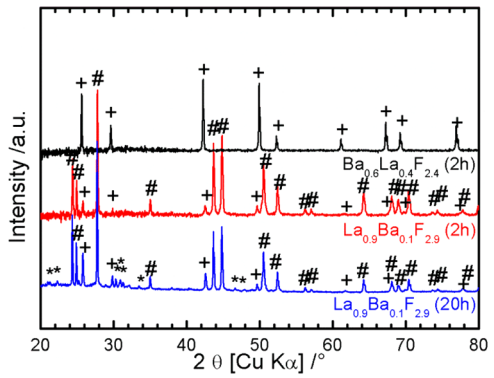

Figure 5. XRD patterns of the pressed pellets after sintering at 800 °C. (+) BaF_2-based phase with a fluorite-type structure, (#) LaF_3-based phase with a tysonite-type structure and (*) contaminations (see Table 2).

fluorite-type compound, only one phase was detected corresponding to the respective solid solution with a fluorite-type structure. The cell parameters remained unchanged compared to the as-milled samples, indicating that the heat treatment only leads to grain growth. For $La_{0.9}Ba_{0.1}F_{2.9}$, two phases were observed in the XRD pattern. One with a tysonite-type structure $La_{1-y}Ba_yF_{3-y}$ having cell parameters slightly smaller than the tysonite-type phase obtained after milling and the second with a fluorite-type structure very similar to the samples $Ba_{1-x}La_xF_{2+x}$. Comparing the cell parameters determined here (Table 2) with those measured for different concentrations after milling (Table 1 and ref 18), we can approximate $y = 0.05$ and $x = 0.5$ for the phases obtained after sintering. It looks as if the solid solution was demixing during the heat treatment, although the phase diagram LaF_3–BaF_2 indicates a solubility limit for BaF_2 in the tysonite structure of 14 mol %,[41] which is above the starting concentration of the sample. This demixing was also observed after 20 h of heat treatment. In addition for this sample, we observed a significant contamination probably coming from the quartz tube with the formation of oxide (La_2O_3, reference ICSD 56771) and silicate compounds ($La_{9.33}(SiO_4)_6O_2$, reference ICSD 154068).

The samples $Ba_{0.6}La_{0.4}F_{2.4}$ and $La_{0.9}Ba_{0.1}F_{2.9}$ after 2 h of sintering were also analyzed by NMR, and the results are given in Figure 6. The spectra are composed of the similar main spectral features described above with a single peak at −24 and

dx.doi.org/10.1021/am4052188 | ACS Appl. Mater. Interfaces 2014, 6, 2103−2110

Table 2. Results of Rietveld Refinements and Conductivity Parameters for $La_{0.9}Ba_{0.1}F_{2.9}$ and $Ba_{0.6}La_{0.4}F_{2.4}$ after Sintering at 800 °C[a]

Compound	$La_{0.9}Ba_{0.1}F_{2.9}$	$La_{0.9}Ba_{0.1}F_{2.9}$	$Ba_{0.6}La_{0.4}F_{2.4}$
sintering time (h)	2	20	2
phases	$La_{1-y}Ba_yF_{3-y}$ (t)	$La_{1-y}Ba_yF_{3-y}$ (t)	$Ba_{0.6}La_{0.4}F_{2.4}$
	$Ba_{1-x}La_xF_{2+x}$ (f)	$Ba_{1-x}La_xF_{2+x}$ (f)	
		La_2O_3	
		$La_{9.33}(SiO_4)_6O_2$	
cell parameters (Å)	a = 7.21, c = 7.37 (t)	a = 7.20, c = 7.36 (t)	a = 6.07
	a = 6.04 (f)	a = 6.02 (f)	
crystallite size (Å)	78 (t)	186 (t)	72
	39 (f)	109 (f)	
σ_{DC} at 160 °C (S·cm^{-1})	9.06×10^{-4}	8.3×10^{-4}	5.08×10^{-5}
E_a (eV)	0.39	0.40	0.52
σ_0 (S·K·cm^{-1})	1.36×10^4	1.59×10^4	2.46×10^4
ΔH_m (eV)			0.49
f_0 (Hz)			5.57×10^{12}

[a]The (t) and (f) letters indicate values obtained for the tysonite- and the fluorite-type phases, respectively (see the Results and Discussion).

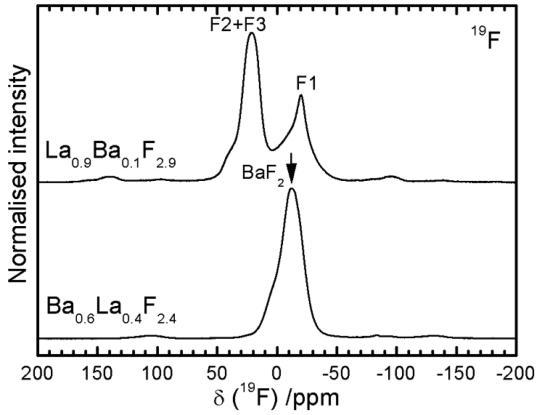

Figure 6. ^{19}F spectra of the two sintered samples (2 h). The main spectral features of LaF_3 and BaF_2 are visible: main peaks around −24, +20 (double peak) and −14 ppm, respectively.

a double (broad) peak centered around 20 ppm for $La_{0.9}Ba_{0.1}F_{2.9}$ and a peak at −14 ppm for $Ba_{0.6}La_{0.4}F_{2.4}$. The lines are narrower features than before sintering, which is in agreement with the increased ordering of the structure expected after heat treatment and the removal of grain boundaries. In the spectrum of $Ba_{0.6}La_{0.4}F_{2.4}$, two peaks can be distinguished: one for BaF_2 (at −14 ppm) and the other as the average of the four interstitial sites originated from LaF_3 doping.[18] In contrast to that, for $La_{0.9}Ba_{0.1}F_{2.9}$, in addition to the two peaks at ca. −24 and +20 ppm already obtained after milling (Figure 2), higher shift resonances at −14 and +38 ppm are observed. The shoulder around −14 ppm may correspond to the contribution of F anions from the BaF_2-based fluorite-type compound that was found by XRD. The origin of the broader shoulder at ca. +38 ppm is not very clear but probably corresponds to F anions from more disordered regions. Comparison of the different T_1 relaxation times for the as-milled and sintered $La_{0.9}Ba_{0.1}F_{2.9}$ samples is given in Figure S1 (Supporting Information) and shows that the bulk conductivity of the sintered sample is much higher than for the other compounds.

The impedance spectra for the fluorite-type sample $Ba_{0.6}La_{0.4}F_{2.4}$ have a similar shape to what was measured on the as-milled material with one semicircle at high frequencies and a straight line at low frequencies (see the Supporting Information, Figure S3).[18] The resistance of the semicircle was taken to calculate the ionic conductivity in this sample (Figure 7). It was also possible to perform an analysis of the AC

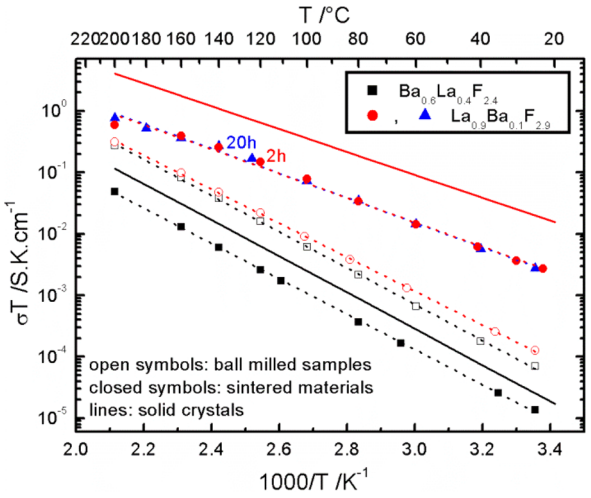

Figure 7. Arrhenius plot of the conductivities for the as-milled and sintered samples $La_{0.9}Ba_{0.1}F_{2.9}$ (○ as-milled, ● sintered for 2 h and ▲ sintered for 20 h) and $Ba_{0.6}La_{0.4}F_{2.4}$ (□ as-milled and ■ sintered for 2 h). Values reported in the literature for single crystals (solid lines) are given for comparison.[21] The dotted lines represent the linear fit obtained for calculating the activation energies.

conductivity to extract the defect migration parameters as was done for the as-milled samples. The results are given in Table 2. The activation energies were almost unchanged after sintering for $Ba_{0.6}La_{0.4}F_{2.4}$, but we observed a decrease of the conductivity values after sintering. This behavior can be easily explained by the reduced grain boundary fraction in the sample after grain growth. We already demonstrated[18] that for this sample, the ionic conductivity is controlled by the migration of vacancies along the grain boundaries. For bigger grains, fewer migration paths are available compared to the as-milled samples, this is illustrated by the lower attempt frequency calculated for the sintered samples. The attempt frequency is related to the frequency of vibration in the lattice,[34] here probably in the boundaries, which may be smaller when the boundaries fraction is reduced.

For $La_{0.9}Ba_{0.1}F_{2.9}$, some changes created by the sintering treatment appear already in the impedance spectra (Figure 3a,b). First, the resistances are much lower than for the as-milled sample, indicating a much higher conductivity in the sintered sample. In addition, three semicircles and one straight line are obtained in the impedance spectrum at 30 °C, the first semicircle at high frequencies disappears and the straight line at low frequencies becomes a semicircle at 100 °C. El Omari et al.[42] have reported the presence of three semicircles in the impedance spectrum of sintered $Ln_{1-y}Cd_yF_{3-y}$ samples (Ln = Ce, Nd). They attributed these semicircles to bulk, grain boundaries and electrodes properties when decreasing the frequency, respectively. However, for the $La_{0.9}Ba_{0.1}F_{2.9}$ samples here, fitting the spectra with the equivalent circuit given in Figure 3d indicates that the two semicircles at high frequencies have capacitances values in the range of grain boundary

dx.doi.org/10.1021/am4052188 | ACS Appl. Mater. Interfaces 2014, 6, 2103−2110

phenomena (labelled GB1 and GB2, see the Supporting information, Table S2).[36] Nevertheless, the capacitance obtained for the first semicircle (ca. 8×10^{-11} F) is lower to what we found for the as-milled samples (1×10^{-10} to 5×10^{-10} F) but higher than the values given by El Omari et al.[42] The semicircle at lower frequencies and the straight line (or the two semicircles at lower frequencies) correspond to electrode phenomena (labelled E1 and E2). Note that similar impedance spectra were obtained for the sample after 20 h of sintering. For the reactions at the electrodes, we assume that in addition to the electrode polarization already observed for the ball-milled sample (straight line), there is a contribution of the surface of the pellet that may be modified by the heat treatment, e.g., some contamination may occur at the surface (pyrolysis, adsorption). The capacitances values obtained are in good agreement with surface layer phenomena (Supporting Information, Table S2).[36]

To calculate the ionic conductivity of the sintered samples given in Figure 7, we considered the contributions of the two semicircles at the highest frequencies and added the resistances of both to obtain the electrolyte resistance. It was not possible to perform the AC conductivity analysis for these samples because both contributions GB1 and GB2 could not be separated; therefore, it was not possible to determine the hopping frequency. Thus, the activation energy given in Table 2 represents the overall ionic conductivity adding the two grain boundary contributions. The value obtained is close to that given for single crystal although the activation energy in Table 2 should be a combination of two conduction mechanisms. Moreover, the conductivity values are still lower than for the single crystal. The grain boundaries still act as barrier to the conduction but their effect is reduced because of their lower fraction in the sample. To better understand the origin of these two contributions, we plotted the conductivities calculated for each semicircle (Figure 8). The conductivities calculated at different temperatures for the semicircle at higher frequencies (GB1) closely follow the conductivity values reported for single crystals.[21] It seems that the first semicircle obtained by impedance spectroscopy actually corresponds to the bulk conductivity. For lower temperatures (<120 °C), the activation energy is 0.39 eV, which is in good agreement to the value reported for doped-LaF_3 (see Table 1). Still, there is discrepancy to the bulk core dominated NMR values, which are lower than 0.3 eV. The value obtained for the second semicircle (GB2) is 0.42 eV (T < 120 °C).

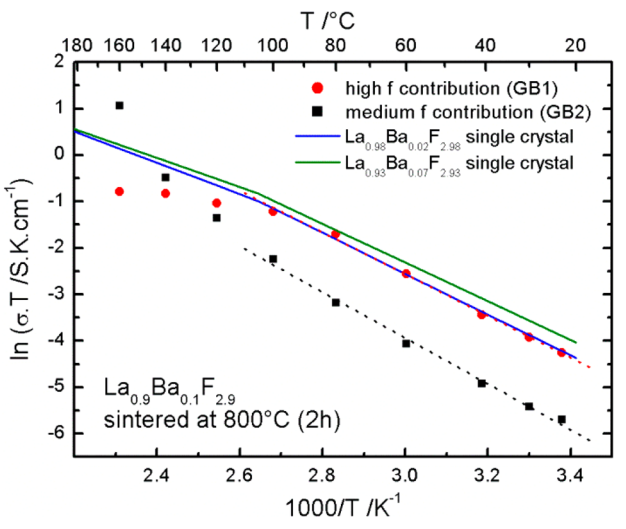

Figure 8. Arrhenius plot for the conductivities calculated for each semicircle obtained by impedance spectroscopy for the sample $La_{0.9}Ba_{0.1}F_{2.9}$ sintered at 800 °C (2 h). The dotted lines represent the linear fit obtained for calculation of activation energies.

The question is then why the capacitances values measured are much higher than usually reported for bulk phenomena. In fact, the contribution of each phenomenon is dependent of the thickness of the corresponding region of a polycrystalline system.[37] Therefore, bulk phenomena have usually very low capacitances because of the relative large volume fraction of the grains. However, in our samples, even after sintering, the grains are still relatively small (<100 nm), which may explain the higher capacitances values obtained. For example, the grain sizes in the samples studied by El Omari et al.[42] are probably much bigger than in our sample because they sintered much coarser materials. From these results, it appears that it is possible to drastically reduce the resistance of the grain boundaries and improve the conductivity in $La_{0.9}Ba_{0.1}F_{2.9}$ samples by sintering. Note that the effect of the presence of a second fluorite-type phase in the sample is difficult to separate here. Its contribution to the conductivity is probably added to the general grain boundaries contribution (GB2).

Therefore, we tried to sinter $La_{0.9}Ba_{0.1}F_{2.9}$ for a longer time (20 h) to further reduce the fraction of grain boundaries and thus, hopefully improve the ionic conductivity to even higher values. Unfortunately, the conductivity values measured after 20 h of sintering are very close to those obtained after only 2 h (Figure 7) The Rietveld refinement of the XRD pattern confirms the larger crystallite size (>100 nm) after longer sintering time but the expected improvement of the conductivity may be hindered by the presence of contamination in the sample (Table 2 and Figure 5). The presence of oxides, silicates and likely the fluorite-type phase may create additional boundaries in the sample (as done by adding oxides to fluorite-type fluorides by doping)[43] that still act as barrier for fast ionic conduction.

4. CONCLUSION

The study of the ionic conductivity in $La_{1-y}Ba_yF_{3-y}$ solid solutions having a tysonite-type structure shows that the mechanism of conductivity is rather different to what is described for fluorite-type samples. For as-milled materials, the conductivity that proceeds by the migration of vacancies through the sample is partly blocked by the presence of grain boundaries. The activation energies obtained are higher than those obtained from T_1-NMR investigations. They are also higher than the values which have been reported for single crystals but are not so different from those found in doped-BaF_2 samples. This activation energy may be representative of vacancy migration along the grain boundaries. Therefore, sintering treatments of the samples to reduce grain boundaries and induce grain growth obviously lead to an improvement of the ionic conductivity as is shown for $La_{0.9}Ba_{0.1}F_{2.9}$. However, the conductivity mechanism becomes more complicated after sintering as two obvious contributions, one from the bulk and the other from the grain boundaries can be detected by impedance. Still there might be the contribution from the core bulk visible from NMR. An attempt to further improve the conductivity using longer sintering time did not lead to further improvement of the conductivity likely because of the presence additional (minor) phases that contribute to the boundaries

dx.doi.org/10.1021/am4052188 | ACS Appl. Mater. Interfaces 2014, 6, 2103−2110

blocking effect. Additional studies trying to remove contamination or using lower quantity of dopant to avoid demixing are on-going to further improve the ionic conductivity.

■ ASSOCIATED CONTENT

Supporting Information

Average T_1 relaxation times calculated from NMR for the two sintered samples compared to other compounds. Impedance spectra (Nyquist plots) of the as-milled and sintered $Ba_{0.6}La_{0.4}F_{2.4}$ samples at 25 °C and 120 °C. Results of impedance spectra fitting for the as-milled and sintered $La_{1-y}Ba_yF_{3-y}$ and $Ba_{0.6}La_{0.4}F_{2.4}$ samples. This material is available free of charge via the Internet at http://pubs.acs.org.

■ AUTHOR INFORMATION

Corresponding Author

*C. Rongeat. E-mail: carine.rongeat@kit.edu. Phone: +49-721-608-28925.

Notes

The authors declare no competing financial interest.

■ ACKNOWLEDGMENTS

Financial support by State of Baden-Wurttemberg, Project house e-drive (#PHed.L.0208.01) is gratefully acknowledged. We are greatly thankful to European Social Fund, Estonian Research Council, TUT and KBFI for support and financing projects MTT68, SF0690034s09, PUT126 and B618.

■ REFERENCES

(1) Bruce, P. G.; Scrosati, B.; Tarascon, J. M. *Angew. Chem., Int. Ed.* **2008**, *47*, 2930−46.
(2) Goodenough, J. B.; Park, K.-S. *J. Am. Chem. Soc.* **2013**, *135*, 1167−76.
(3) Cabana, J.; Monconduit, L.; Larcher, D.; Palacín, M. R. *Adv. Mater.* **2010**, *22*, E170−92.
(4) Fichtner, M. *J. Alloys Compd.* **2011**, *509*, S529−S534.
(5) Hartmann, P.; Bender, C. L.; Vračar, M.; Dürr, A. K.; Garsuch, A.; Janek, J.; Adelhelm, P. *Nat. Mater.* **2013**, *12*, 228−32.
(6) Mohtadi, R.; Matsui, M.; Arthur, T. S.; Hwang, S.-J. *Angew. Chem., Int. Ed.* **2012**, *51*, 9780−3.
(7) Zhao, X.; Ren, S.; Bruns, M.; Fichtner, M. *J. Power Sources* **2013**, *245*, 706−711.
(8) Anji Reddy, M.; Fichtner, M. *J. Mater. Chem.* **2011**, *21*, 17059−17062.
(9) Sorokin, N. I.; Sobolev, B. P. *Crystallogr. Rep.* **2007**, *52*, 842−863.
(10) Patro, L. N.; Hariharan, K. *Solid State Ionics* **2013**, *239*, 41−49.
(11) Schoonman, J.; Oversluizen, G.; Wapenaar, K. E. D. *Solid State Ionics* **1980**, *1*, 211−221.
(12) Saito, Y.; Maier, J. *J. Electrochem. Soc.* **1995**, *142*, 3078−3083.
(13) Bollmann, W. *Phys. Status Solidi A* **1973**, *18*, 313−321.
(14) Barsis, E.; Taylor, A. *J. Chem. Phys.* **1968**, *48*, 4362−4367.
(15) Wapenaar, K. E. D.; van Koesveld, J. L.; Schoonman, J. *Solid State Ionics* **1981**, *2*, 145−154.
(16) Puin, W.; Rodewald, S.; Ramlau, R.; Heitjans, P.; Maier, J. *Solid State Ionics* **2000**, *131*, 159−164.
(17) Düvel, A.; Kuhn, A.; Robben, L.; Wilkening, M.; Heitjans, P. *J. Phys. Chem. C* **2012**, *116*, 15192−15202.
(18) Rongeat, C.; Reddy, M. A.; Witter, R.; Fichtner, M. *J. Phys. Chem. C* **2013**, *117*, 4943−4950.
(19) Sorokin, N. I.; Sobolev, B. P. *Phys. Solid State* **2008**, *50*, 416−421.
(20) Privalov, A. F.; Vieth, H. M.; Murin, I. V. *J. Phys.: Condens. Matter* **1994**, *6*, 8237−8243.
(21) Roos, A.; van de Pol, F. C. M.; Keim, R.; Schoonman, J. *Solid State Ionics* **1984**, *13*, 191−203.
(22) Sorokin, N. I.; Breiter, M. W. *Solid State Ionics* **1997**, *99*, 241−250.
(23) Omari, M.; El Senegas, J.; Reau, J.-M. *Solid State Ionics* **1998**, *107*, 293−305.
(24) Murin, I. V.; Glumov, O. V.; Amelin, Y. V. *J. Appl. Chem. USSR* **1980**, *53*, 1132−1135.
(25) Sorokin, N. I.; Krivandina, E. A.; Zhmurova, Z. I.; Sobolev, B. P.; Fominykh, M. V.; Fistul, V. V. *Phys. Solid State* **1999**, *41*, 573−575.
(26) Sobolev, B. P. *Crystallogr. Rep.* **2012**, *57*, 434−454.
(27) Sobolev, B. P.; Sviridov, I. A.; Fadeeva, V. I.; Sul'yanov, S. N.; Sorokin, N. I.; Zhmurova, Z. I.; Khodos, I. I.; Avilov, a. S.; Zaporozhets, M. a. *Crystallogr. Rep.* **2008**, *53*, 868−880.
(28) Kumar, D. A.; Selvasekarapandian, S.; Nithya, H.; Hema, M. *Ionics* **2012**, *18*, 461−471.
(29) Lutterotti, L. The MAUD program, http://www.ing.unitn.it/~maud/, 2011.
(30) Bondarenko, A. S.; Ragoisha, G. A. EIS Spectrum Analyser, http://www.abc.chemistry.bsu.by/vi/analyser/, 2008.
(31) Farrington, C. G. *Sens. Actuators* **1981**, *1*, 329−346.
(32) Almond, D. P.; West, A. R. *Solid State Ionics* **1983**, *9&10*, 277−282.
(33) Hairetdinov, E. F.; Uvarov, N. F.; Reau, J.-M.; Hagenmuller, P. *Phys. B* **1998**, *244*, 201−206.
(34) Smart, L.; Moore, E. In *Solid State Chemistry: An Introduction*; 3rd Ed.; CRC Press: Boca Raton, FL, 2005; pp 201−280.
(35) Huggins, R. A. In *Advanced Batteries: Materials Science Aspects*; Springer: New York, 2009; pp 393−431.
(36) Irvine, J. T. S.; Sinclair, D. C.; West, A. R. *Adv. Mater.* **1990**, *2*, 132−138.
(37) Sinclair, D. C. *Bol. Soc. Esp. Ceram. Vidrio* **1995**, *65*, 55−66.
(38) Stebbins, J. F.; Zeng, Q. *J. Non-Cryst. Solids* **2000**, *262*, 1−5.
(39) Sadoc, A.; Body, M.; Legein, C.; Biswal, M.; Fayon, F.; Rocquefelte, X.; Boucher, F. *Phys. Chem. Chem. Phys.* **2011**, *13*, 18539−50.
(40) Ivanov-Shits, A. K.; Sorokin, N. I.; Fedorov, P. P.; Sobolev, B. P. *Solid State Ionics* **1989**, *31*, 269−280.
(41) Sobolev, B. P.; Tkachenko, N. L. *J. Less-Common Met.* **1982**, *85*, 155−170.
(42) Omari, M.; El Senegas, J.; Reau, J.-M. *Solid State Ionics* **1998**, *107*, 281−291.
(43) Fujitsu, S.; Miyayama, M.; Koumoto, K.; Yanagida, H.; Kanazawa, T. *J. Mater. Sci.* **1985**, *20*, 2103−2109.